

Nonlinear MHD Simulations in the Large Helical Device

MIURA Hideaki*, HAYASHI Takaya and SATO Tetsuya

National Institute for Fusion Science, Oroshi-cho 322-6, Toki, Gifu 509-5292, Japan

(Received: 5 December 2000 / Accepted: 27 August 2001)

Abstract

A new simulation code to solve fully nonlinear, resistive magnetohydrodynamic (MHD) equations in a full three-dimensional geometry, which has seldom been attempted, is developed to investigate pressure-driven phenomena in helical devices. Simulations for the geometry of the Large Helical Device (LHD) show growth and nonlinear saturation of pressure-driven instabilities. These results show that our new code is applicable to investigate nonlinear evolution of an MHD plasma in helical devices.

Keywords:

LHD, nonlinear MHD simulation, pressure-driven instability, three-dimensional geometry

1. Introduction

MHD properties of plasmas in helical devices have been extensively studied so far both analytically and numerically. However, nonlinear MHD simulations in a full three-dimensional (3D) geometry of a helical device, as addressed in this paper, has seldom been attempted until now, except for a preliminary trial. [1] Properties of instabilities, the ballooning mode in particular, are sensitive to the 3D geometry of equilibrium configuration, such as the local magnetic curvature and the local magnetic shear. Thus, a two-dimensional treatment of helical plasmas, such as the averaging method, is insufficient for complete elucidation of MHD behaviors. With the remarkable progress in the recent computer performance, execution of this kind of time-consuming nonlinear simulation in a solid configuration became feasible. In this paper, we develop a new simulation code for helical plasmas based on Hayashi's code [1], and report some distinct phenomena observed by using the code. The results indicate applicability of our code to investigate time-evolution of various MHD phenomena in realistic geometry of helical devices.

2. Simulation Code

Our simulation code solves fully-nonlinear, compressible and resistive MHD equations in a full 3D geometry. The equation system is described as

$$\frac{\partial \rho}{\partial t} = -\nabla \cdot (\rho \mathbf{v}), \quad (1)$$

$$\rho \left(\frac{\partial \mathbf{v}}{\partial t} + \mathbf{v} \cdot \nabla \mathbf{v} \right) = -\nabla p + \mathbf{j} \times \mathbf{B} + \mu \left[\nabla^2 \mathbf{v} + \frac{1}{3} \nabla (\nabla \cdot \mathbf{v}) \right], \quad (2)$$

$$\frac{\partial p}{\partial t} + \mathbf{v} \cdot \nabla p = -\gamma p \nabla \cdot \mathbf{v} + (\gamma - 1) (\eta \mathbf{j} \cdot \mathbf{j} + \Phi - \nabla \cdot \mathbf{q}), \quad (3)$$

$$\frac{\partial \mathbf{B}}{\partial t} = -\nabla \times (-\mathbf{v} \times \mathbf{B} + \eta \mathbf{j}), \quad (4)$$

$$\mathbf{j} = \nabla \times \mathbf{B}, \quad (5)$$

*Corresponding author's e-mail: miura@toki.theory.nifs.ac.jp

$$e_{ij} = \frac{1}{2} \left(\frac{\partial v_i}{\partial x_j} + \frac{\partial v_j}{\partial x_i} \right), \quad (6)$$

$$\Phi = 2\mu \left[e_{ij} e_{ji} - \frac{1}{3} (\nabla \cdot \mathbf{u})^2 \right] \quad (7)$$

$$\mathbf{q} = -\kappa \nabla \left(\frac{p}{\rho} \right), \quad (8)$$

where ρ , \mathbf{v} , p , \mathbf{B} , \mathbf{j} , e_{ij} and \mathbf{q} are the mass density, velocity vector, pressure, magnetic field vector, current vector, (i,j) component of the strain-rate-tensor and heat flux, respectively. Symbols η , κ , μ are the resistivity, conductivity and shear viscosity, respectively. These dissipative coefficients are assumed to be isotropic constants.

The MHD equations (1)–(8) are made non-dimensional by the use of the toroidal Alfvén time τ_A and other quantities in the same manner with the HINT code [2], which obtains a 3D finite-pressure equilibrium state. The equations are defined on the “helical-toroidal” coordinate (u^1, u^2, u^3) . Refer to Harafuji *et al.* [2] on the coordinate system used in this code, mathematical expressions for metrics, nature of numerical grids and so on. Here we set parameters to simulate plasmas in the LHD geometry [3,4] which is a heliotron type stellarator with the pitch period number $M = 10$ and the pole number $l = 2$. Behavior of a plasma in the half pitch period of the torus in the toroidal direction is solved numerically by imposing the stellarator symmetry to the system. (The lowest toroidal mode n is 10.) The initial 3D equilibrium solution is computed by the HINT code. Equations (1)–(8) are discretized by using the fourth-order central-finite-difference scheme and integrated in the time direction by the Runge-Kutta-Gill scheme. The ratio of specific heats is $\gamma = 5/3$. Control parameters $\kappa = 1 \times 10^{-6}$ and $\mu = 2 \times 10^{-3}$ are fixed throughout this article. The resistivity $\eta = 1.73 \times 10^{-6}$ is also fixed as far as we do not describe the value explicitly. Number of the grid points are 97×97 on a poloidal section and 32 in the toroidal direction. Dependency of plasma behaviors on different η values and other informations should be seen in our next article. [5]

3. Observation of Linear Instabilities

In this section we study growth of linear instabilities. First, we conduct a simulation (Run-1) for an initial equilibrium with major radius of the vacuum

magnetic axis $R_{ax} = 3.7$ m in the dimensional quantity (the major radius of the center of the helical coil of LHD is 3.9 m) and central beta $\beta_0 = 4\%$. In Fig. 1(a), the rotational transform (t) of this equilibrium is shown. A calculation of the specific volume shows that the core part of the configuration has a property of magnetic well

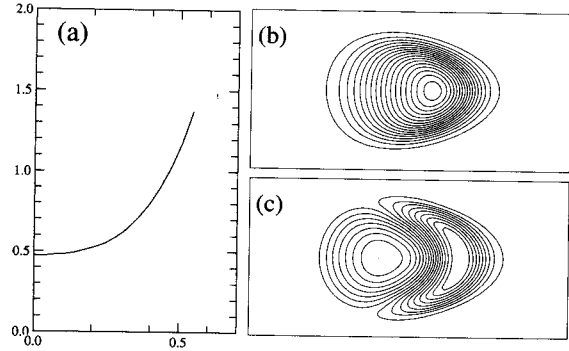


Fig. 1 (a) Rotational transform, contour plots of (b) the pressure and (c) toroidal current (Pfirsch-Schlüter current) on the horizontally-elongated poloidal section.

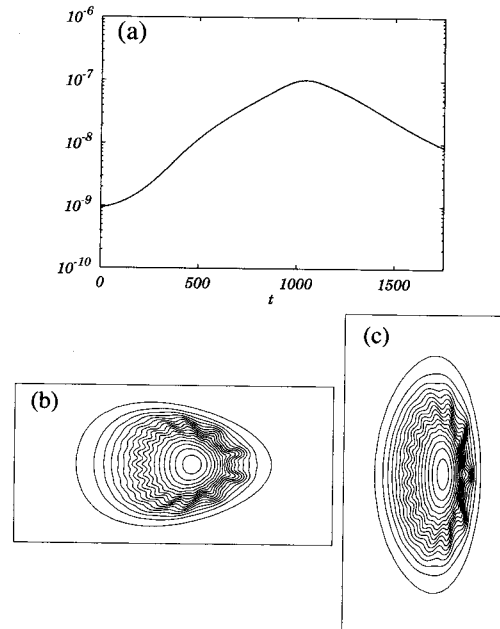


Fig. 2 (a) Evolution of the total kinetic energy in a nonlinear MHD simulation Run-1. The time was shifted to the time when the kinetic energy begins an exponential growth. Contour plots of the pressure on a (b) horizontally- and (c) vertically-elongated poloidal sections at $t \approx 1000 \tau_A$. The right-hand side of this figure is associated with the outer side of the the LHD torus.

while the edge region is magnetic hill. Figures 1(b) and (c) are contour plots of the pressure and toroidal current (Pfirsch-Schlüter current) on the horizontally-elongated poloidal section, respectively. Throughout this article, the outer side of the torus is in the right hand side when we see contour plots of any quantity. The initial pressure profile for the HINT computation is given by $p(\psi) = (1 - \psi)^2$ (peaked profile), where ψ represents the toroidal flux function. According to a previous study, this plasma equilibrium is weakly Mercier-unstable in the steep pressure gradient region. [6] (Refer also to Chen *et al.* [7] for properties of an ideal ballooning instability on a Mercier-unstable heliotron system).

In Fig. 2(a), evolution of the kinetic energy obtained in the Run-1 simulation is shown. The kinetic energy is integrated over the entire volume. In what follows we pay our attention to the kinetic energy because we start from an initial equilibrium with small perturbed velocity and growth of the kinetic energy represents growth of an instability clearly. Contour plots

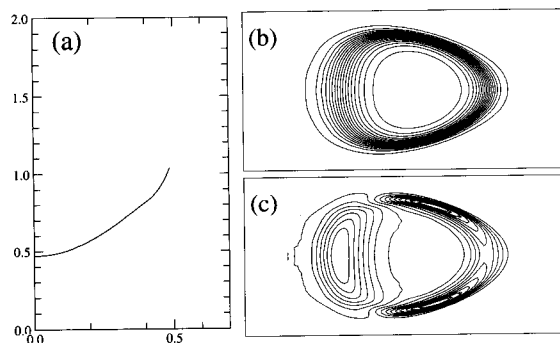


Fig. 3 Initial condition of a simulation with a flat pressure profile. (a) Rotational transform, contour plots of (b) the pressure and (c) toroidal current on the horizontally-elongated poloidal section.

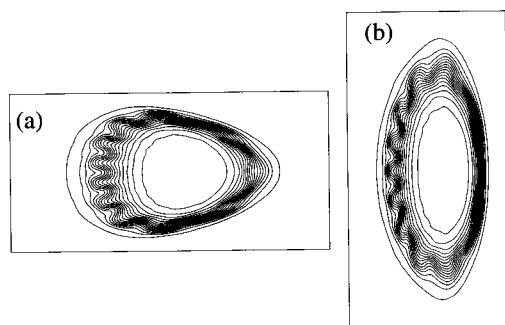


Fig. 4 Contour plots of the pressure on (a) horizontally- and (b) vertically-elongated poloidal sections.

of the pressure at $t = 425 \tau_A$ on the horizontally- and vertically-elongated poloidal sections are shown in Figs. 2(b) and (c), respectively. Columnar deformations of contours are observed at a region $t \approx 2/3$. The most dominant poloidal and toroidal mode number are $m = 15$ and $n = 10$, respectively. The largest deformations are observed in the outer sides of the torus, and they are clearer in Fig. 2(b) than in Fig. 2(c). Recall that destabilization effect of the magnetic curvature is the strongest on the horizontally-elongated poloidal section. Furthermore, a parameter survey for a range of the resistivity $1 \times 10^{-6} \leq \eta \leq 3.16 \times 10^{-4}$ reveals that the growth rate depends on the resistivity, roughly proportional to $\eta^{1/3}$. [5] These results show that the instability observed in Figs. 2 is the resistive ballooning instability.

In Figs. 2(b) and (c), we observe large columnar deformations in the outer side of the torus. In order to see a property of instability in other cases, we conduct a simulation (Run-2) by using a initial equilibrium with a broader pressure profile $p(\psi) = (1 - \psi^4)^2$, magnetic axis $R_{ax} = 3.7$ m and $\beta_0 = 4\%$. In Fig. 3, the rotational transform, contour plots of the pressure and toroidal current on the horizontally-elongated poloidal section are shown. Since this equilibrium contains larger internal pressure energy compared with an equilibrium shown in Figs. 1 and has the steepest pressure gradient at the magnetic hill region in the edge, a linear analysis predicts appearance of unstable interchange instability rather than ballooning instability with this equilibrium.

In Run-2, an exponential growth and saturation of the kinetic energy similar to those in Fig. 2(a) is observed (figure is omitted). The growth rate is slightly greater than that observed in Run-1. In Fig. 4, contour plots of the pressure on horizontally- and vertically-elongated poloidal sections at the time when the kinetic energy is under its exponential growth are shown. Deformations of the pressure are observed at a region $t \approx 0.77$, with the most dominant mode being $m/n = 13/10$. These deformations are observed all around the plasma core and magnitude of the deformations looks similar each other. Furthermore, we do not observe clear difference in the magnitude of deformations between Fig. 4(a) and Fig. 4(b). Thus an instability which brought this deformation should be identified as the interchange instability rather than the ballooning instability.

Results of Run-1 and Run-2 in this section show that our new code simulates linear growth of ballooning and interchange instabilities appropriately in consistent

with previous researches [6,8]. These results, in linear stage of an instability, are checked with larger number of grid points. [5]

4. Nonlinear Saturation and Pressure Profile

The advantage of the approach described in this paper is the capability of tracing the time-evolution down to the nonlinear stage, in particular the saturation level of the excited modes. The kinetic energy of Run-1 shown in Fig. 2(a) saturates at $t \approx 1000 \tau_A$ due to the nonlinearity of the MHD equations (1)–(8), and begins to decrease. Evolution of the kinetic energy of Run-2 also saturates due to the nonlinearity.

In order to see pressure profiles of these two simulations in their nonlinear stages, birds' eyes views of the pressure on the horizontally-elongated poloidal section at their saturation times are shown in Fig. 5. In Figs. 5(a) and (b), a birds' eyes view of the pressure of Run-1 and Run-2 observed from the outer side of the torus is shown, respectively. In Fig. 5(a), we observe that ridges of pressure are formed. These long, curved ridges toward the outer side of torus are formed by the ballooning instability. After the linear growth is saturated at this time, these steep ridge structures are gradually fall down to less-steep, gently curving structures in the course of nonlinear relaxation. In Fig. 5(b), on the other hand, we do not see formation of ridges like those in Fig. 5(a). In stead of the ridge structures, we observe structures something like

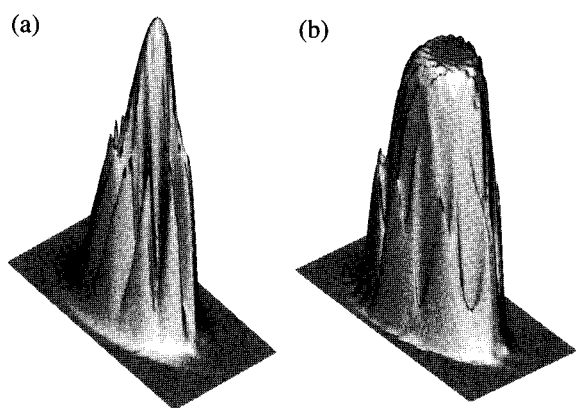


Fig. 5 Birds' eyes' view of the pressure on the horizontally-elongated poloidal section for (a) Run-1 and (b) Run-2.

triangular shields that surround plasma core. These triangular shields are formed by the growth of the interchange instability. It may be noteworthy that both of those ballooning and interchange instabilities with the medium scale toroidal mode number can change plasma profiles significantly and causes appearance of distinct pressure structures in the edge region as are seen in Fig. 5, although not being destructive to destroy the whole plasma.

5. Summary

We have developed a new simulation code to solve a fully-nonlinear, dissipative MHD equations in full 3D geometry of helical plasmas. We observed excitation of either the ballooning or the interchange instability, depending on the initial equilibria, in the linear stages of the simulations. Their behaviors are in consistent with predictions of previous linear stability analysis. We have also shown that instabilities saturate due to nonlinearity. In the course of nonlinear evolutions, the instabilities have changed pressure profiles significantly. Pressure profiles at the saturation time of either the ballooning or the interchange instability have distinct structures in the edge regions, respectively. The characteristic pressure structure caused by the respective instabilities, either ridges or triangular shields, can give information in identifying the nature of unstable mode observed in experiments.

As described above, successful reproduction of linear growth and saturations of instabilities implies that our new code is applicable to analyze nonlinear plasma behaviors in helical devices.

References

- [1] T. Hayashi, *Proc. 3rd Australia-Japan Workshop on Plasma Theory and Computation* (Robertson, 1995) Australia National Univ. Canberra **26** (1995).
- [2] H. Harafuji, T. Hayashi and T. Sato, *J. Comp. Phys.* **81**, 169 (1989).
- [3] S. Sakakibara *et al.*, 18th IAEA Fusion Energy Conference (Sorento, 2000). NIFS Report **652**.
- [4] N. Ohya *et al.*, *Phys. Rev. Lett.* **84**, 103 (2000).
- [5] H. Miura, T. Hayashi and T. Sato, to appear in *Phys. Plasmas*.
- [6] K. Ichiguchi *et al.*, *Nucl. Fusion* **33**, 481 (1993).
- [7] J. Chen *et al.*, *Phys. Plasmas* **6**, 1562 (1999).
- [8] K. Ichiguchi, private communication.